Photoinduced Ferrimagnetic Systems in Prussian Blue Analogues $C^I_xCo_4[Fe(CN)_6]_y$ (C^I = Alkali Cation). 3. Control of the Photo- and Thermally Induced Electron Transfer by the $[Fe(CN)_6]$ Vacancies in Cesium Derivatives

Virginie Escax,[†] Anne Bleuzen,*[,†] Christophe Cartier dit Moulin,[†,‡] Françoise Villain,[†,‡] Antoine Goujon,[§] François Varret,[§] and Michel Verdaguer*[,†]

Contribution from the Laboratoire de Chimie Inorganique et Matériaux Moléculaires, Unité CNRS 7071, Université Pierre et Marie Curie, Bât. F 74, 4 place Jussieu, 75252 Paris Cedex 05, France, Laboratoire pour l'Utilisation du Rayonnement Electromagnétique, UMR CNRS 130-CEA-MENRS, Bât. 209d, Université Paris-Sud, BP34, 91898 Orsay Cedex, France, and Laboratoire de Magnétisme et d'Optique, CNRS-Université de Versailles, UMR 8634, 45 avenue des Etats-Unis, 78035 Versailles Cedex, France

Received May 29, 2001

Abstract: We synthesized a series of CoFe Prussian blue analogues along which we tuned the amount of cesium cations inserted in the tetrahedral sites of the structure. Structure and electronic structure have been investigated, combining XANES, infrared spectroscopy, powder X-ray diffraction experiments, and magnetization measurements. The change of the magnetization induced by light along the series shows that the efficiency of the photoinduced magnetization, evidenced a few years ago in similar compounds by Hashimoto et al. (Sato, O.; Iyoda, T.; Fujishima, A.; Hashimoto, K. *Science* **1996**, *272*, 704−705; Sato, O.; Einaga, Y.; Iyoda, T.; Fujishima, A.; Hashimoto, K. *J. Electrochem. Soc.* **1997**, *144*, L11−L13; Sato, O.; Einaga, Y.; Iyoda, T.; Fujishima, A.; Hashimoto, K. *J. Phys. Chem. B* **1997**, *101*, 3903−3905; Einaga, Y.; Ohkoshi, S.-I.; Sato, O.; Fujishima, A.; Hashimoto, K. *Chem. Lett.* **1998**, 585−586; and Sato, O.; Einaga, Y.; Fujishima, A.; Hashimoto, K. *Inorg. Chem.* **1999**, *38*, 4405−4412), depends on a compromise between the number of excitable diamagnetic pairs and the amount of $[Fe(CN)_6]$ vacancies giving the network flexibility. Besides the efficiency of the photoinduced process, the amount of $[Fe(CN)_6]$ vacancies also controls a thermally induced electron transfer.

Introduction

When Hashimoto and co-workers evidenced a photoinduced magnetization at low temperature in a Co−Fe Prussian blue analogue in 1996, the proposed explanation of this phenomenon was (i) the presence of diamagnetic pairs Co^{III} low spin−Fe^{II} low spin in the compound and (ii) a photoinduced electron transfer from Fe^{II} to Co^{III} to give Co^{II}−Fe^{III} magnetic pairs.[1−7] In part 1 of our work,[8] we showed that to increase the number of Co^{III}−Fe^{II} efficient diamagnetic pairs, one has to increase the ligand field Δ_{Co} around the cobalt ion. The face-centered cubic $Co_4[Fe(CN)_6]_{8/3}\square_{4/3}\cdot nH_2O$ Prussian blue presents intrinsic $[Fe(CN)_6]$ vacancies □ due to the stoichiometry. The insertion of alkali metal cations C^+ in the tetrahedral sites of the structure is accompanied by the filling of the vacancies by the anionic ferricyanide to ensure electroneutrality of the solid. The Δ_{Co} ligand field is therefore enhanced by the substitution of water molecules by N-bonded cyanides belonging to the inserted $[Fe(CN)_6]$:

$$Co_4[Fe(CN)_6]_{8/3}\square_{4/3}\cdot nH_2O + xC^+ + x/3[Fe(CN)_6]^{3-} \rightarrow C_xCo_4[Fe(CN)_6]_y\square_{4-y}\cdot n'H_2O$$

$$\text{with } y = (8 + x)/3$$

It is easy to check that starting with a mean cobalt coordination sphere $Co(NC)_4(OH_2)_2$, one obtains $Co(NC)_{4+x/2}(OH_2)_{2-x/2}$ after insertion of xC^+. Following the structural work of Lüdi and Güdel[9] and usual crystallographic convention, the Wyckoff positions 4a (0, 0, 0) are occupied by cobalt ions and the 4b positions ($^1/_2$, $^1/_2$, $^1/_2$), named hereafter iron sites, are occupied by $[Fe(CN)_6]$ or □ vacancies. The C^+ cations are distributed in positions 8c (($^1/_4$, $^1/_4$, $^1/_4$ and $^3/_4$, $^3/_4$, $^3/_4$). In the same paper,[8] we correlated the amount of diamagnetic pairs to the efficiency of the photoinduced magnetization and showed that the presence of diamagnetic pairs is a necessary condition but not a sufficient one to observe a photoinduced magnetization in those compounds. For the demonstration, we synthesized three compounds with various stoechiometries by adding an excess of various alkali cations during the synthesis: one compound presenting a negligible insertion of alkali cations with formula $K_{0.1}Co_4$-

[†] Université Pierre et Marie Curie.
[‡] Laboratoire pour l'Utilisation du Rayonnement Electromagnétique.
[§] Laboratoire de Magnétisme et d'Optique.

(1) Sato, O.; Iyoda, T.; Fujishima, A.; Hashimoto, K. *Science* **1996**, *272*, 704−705.
(2) Sato, O.; Einaga, Y.; Iyoda, T.; Fujishima, A.; Hashimoto, K. *J. Electrochem. Soc.* **1997**, *144*, L11−L13.
(3) Sato, O.; Einaga, Y.; Iyoda, T.; Fujishima, A.; Hashimoto, K. *J. Phys. Chem. B* **1997**, *101*, 3903−3905.
(4) Einaga, Y.; Ohkoshi, S.-I.; Sato, O.; Fujishima, A.; Hashimoto, K. *Chem. Lett.* **1998**, 585−586.
(5) Sato, O.; Einaga, Y.; Fujishima, A.; Hashimoto, K. *Inorg. Chem.* **1999**, *38*, 4405−4412.
(6) Verdaguer, M. *Science* **1996** , *272*, 698−699.
(7) Bleuzen, A.; Lomenech, C.; Dolbecq, A.; Villain, F.; Goujon, A.; Roubeau, O.; Nogues, M.; Varret, F.; Baudelet, F.; Dartyge, E.; Giorgetti, C.; Gallet, J. J.; Cartier dit Moulin, C.; Verdaguer, M. *Mol. Cryst. Liq. Cryst.* **1999**, *335*, 965−974.
(8) Bleuzen, A.; Lomenech, C.; Escax, V.; Villain, F.; Varret, F.; Cartier dit Moulin, C.; Verdaguer, M. *J. Am. Chem. Soc.* **2000**, *122*, 6648−6652.
(9) Lüdi, A.; Güdel, H. U. *Structure and Bonding*; Springer-Verlag: Berlin, 1973; pp 1−21.

10.1021/ja011296r CCC: $20.00
Published on Web 11/27/2001

$[Fe(CN)_6]_{2.7}\cdot 18H_2O$, one compound containing nearly the maximum of inserted cesium cations with formula $Cs_{3.9}Co_4[Fe(CN)_6]_{3.9}\cdot 13H_2O$ and one compound with an intermediate amount of inserted cation with formula $Rb_{1.8}Co_4[Fe(CN)_6]_{3.3}\cdot 13H_2O$. Used as reference compounds in the following, they are respectively called **R1**, **R2**, and **R3**.[8] In part 2 of our work,[10] we went further in the understanding of the photoinduced electron transfer by studying the electronic structure as well as the local structure around the cobalt atom in the photoinduced excited state of the most efficient photomagnetic sample **R3**. These studies led us to complete the initial Hashimoto's statements as follows. As the photoinduced electron transfer is accompanied with a bond lengthening in the first coordination shell of the cobalt atoms, the inorganic network must be flexible enough to absorb the dilatation of the bonds. The $[Fe(CN)_6]$ vacancies should act as relaxation points of the network strains provoked by irradiation so that their presence in the structure should also be a necessary condition to observe the photoinduced magnetization.[7,8,10] The efficiency of the photoinduced electron transfer should then depend on a compromise between the amount of diamagnetic pairs and $[Fe(CN)_6]$ vacancies. In part 1,[8] we made the demonstration with compounds in which the stoichiometries and the amounts of $[Fe(CN)_6]$ vacancies □ were varying together with the nature of the alkali cations, and then the properties of the compounds may, to some extent, depend on the nature of the alkali cation. Furthermore, the amount of inserted alkali cations was fixed by the nature of the alkali cation.

In the present paper, Part 3, we tune the amount of inserted alkali cations but, to avoid possible effects due to the different nature of the alkali cations, we insert different amounts of the same alkali cation, cesium, and we correlate the amounts of $[Fe(CN)_6]$ vacancies □ and of diamagnetic pairs to the photoinduced magnetization. For that, we synthesized a series of compounds with various and tunable quantities of inserted cesium cations (from 0 to 4 per conventional unit cell). Cesium was chosen since for this cation, the incorporated amount into the Prussian blue structure varies most sensitively with the amount present in the reaction solution. The study was performed with four compounds representative of the series. The structures and electronic structures of the four samples were characterized and correlated to their magnetic properties before and after irradiation.

Experimental Section

Materials and Sample Preparation. Potassium hexacyanoferrate(III) (Fluka, puriss. p.a.), cobalt(II) nitrate (Fluka, p.a.), and cesium nitrate (Aldrich) were used as received. The four compounds were synthesized by addition of 400 mL of a 2.5×10^{-3} mol L^{-1} aqueous solution of potassium hexacyanoferrate(III) to 100 mL of a 5×10^{-2} mol L^{-1} aqueous solution of Co(II) nitrate. To control the insertion of cesium cations in the solid, various concentrations of cesium nitrate were added to the ferricyanide solution. For all the syntheses, the initial pH of the solutions was adjusted to 5 using HNO_3 diluted solutions. The addition rate was regulated to last 3 h. The powders were centrifuged, washed three times with distilled water, and allowed to dry in air, giving the four compounds **1**−**4**.

Compounds **R1, R2,** and **R3** described in the Introduction were used as references. Their synthesis and characterization have been previously described in part 1.[8] Two Prussian blue analogues have been used as standards for magnetic characterization. Their formulas obtained from the elemental analysis are $Co^{II}_4[Co^{III}(CN)_6]_{2.7}\cdot 17H_2O$ and $Zn^{II}_4[Fe^{III}(CN)_6]_{2.7}\cdot 13H_2O$. Their X-ray diffraction patterns are the ones of face-centered cubic Prussian blue analogues.

(10) Cartier dit Moulin, C.; Villain, F.; Bleuzen, A.; Arrio, M.-A.; Sainctavit, P.; Lomenech, C.; Escax, V.; Baudelet, F.; Dartyge, E.; Gallet, J. J.; Verdaguer, M. *J. Am. Chem. Soc.* **2000**, *122*, 6653−6658.

Table 1. Microanalysis Results and Proposed Formula for Compounds **1**, **2**, **3**, and **4** Compared to the Formulas of Compounds **R1** and **R2**

sample	Cs	Co	Fe	C	N	H	O
R1	$K_{0.1}Co_4[Fe(CN)_6]_{2.7}[\square]_{1.3}\cdot 18\ H_2O$						
1	proposed formula: $Cs_{0.3}Co_4[Fe(CN)_6]_{2.8}[\square]_{1.2}\cdot 18H_2O$						
% exp.	2.99	19.29	12.79	16.35	19.21	2.91	26.35
(calc)	(3.34)	(19.75)	(13.10)	(16.91)	(19.72)	(3.04)	(24.13)
2	proposed formula: $Cs_{0.7}Co_4[Fe(CN)_6]_{2.9}[\square]_{1.1}\cdot 16H_2O$						
% exp.	7.11	18.14	12.55	16.01	18.93	2.48	24.78
(calc)	(7.54)	(19.10)	(13.12)	(16.94)	(19.75)	(2.61)	(20.74)
3	proposed formula: $Cs_{1.2}Co_4[Fe(CN)_6]_{3.2}[\square]_{0.8}\cdot 16H_2O$						
% exp.	11.35	16.40	12.10	16.18	18.56	2.59	23.15
(calc)	(11.71)	(17.31)	(13.12)	(16.93)	(19.75)	(2.37)	(18.79)
4	proposed formula: $Cs_{2.3}Co_4[Fe(CN)_6]_{3.4}[\square]_{0.6}\cdot 14H_2O$						
% exp.	19.38	15.00	10.95	15.12	17.98	1.84	19.63
(calc)	(20.19)	(15.57)	(12.54)	(16.18)	(18.87)	(1.86)	(14.79)
R2	$Cs_{3.9}Co_4[Fe(CN)_6]_{3.9}[\square]_{0.1}\cdot 13H_2O$						

Characterization. Elemental analysis of Co, Fe, C, N, K, H, and Cs was performed at the CNRS analysis facility in Vernaison (the oxygen was assumed to be the only other element, and its content was obtained by difference to 100%). For each compound, a chemical formula, taking into account the weight percentage of each element, the electroneutrality, and the chemistry of the system is proposed. The error bar in the stoichiometric coefficients can be evaluated as 0.1.

Infrared spectra of the powders dispersed in Nujol were recorded at room temperature, over the range 4000−250 cm^{-1} with a Fourier transform spectrometer (Bio-Rad FTS 165).

X-ray absorption near edge spectroscopy (XANES) measurements were performed at the Co and Fe K edges in transmission mode on the XAS 13 beam line at the French synchrotron facility DCI at LURE (Orsay), using Si 311 double monochromator, at room temperature. The energy calibration was checked by recording the spectra of the samples and the metallic (cobalt or iron) foil at the same time. Samples were ground and homogeneously dispersed in cellulose pellets. XANES spectra were recorded with 0.3 eV steps and their absorbances normalized at the middle of the first EXAFS oscillation.

X-ray powder diffraction patterns (Co K_α) were collected with a Philips diffractometer. All diffractograms were recorded over the 5−40° range with a 0.01° step.

Magnetization measurements were performed in a SQUID magnetometer (Quantum Device MPMS5) operating in the alternative mode, equipped with an optical fiber made of multiwire silica. The fiber was connected to a broadband source of light (tungsten halogen lamp, 100 W), through interferential filters (100 nm bandwidth). A cutoff filter provided a large intensity in the range 750 nm ± 50 nm. The power received by the irradiated sample is typically $P = 60$ mW cm^{-2}. The magnetization data for each sample were obtained as follows. In a first step, the magnetization of about 30 mg of powder was measured over the range 5−300 K in the heating mode, using a 100 G applied field. Then, the magnetization of about 3 mg of the sample (pellet-shaped) was measured as a function of the temperature over the 10−300 K range, using a 500 G field. The pellet was then irradiated during 2 h at 10 K. The magnetization was measured during the irradiation period. After irradiation, the magnetization of the irradiated sample was measured as a function of the temperature from 10 to 300 K.

Results and Discussion

Elemental Analysis. The chemical formulas of the four compounds **1**−**4**, given for a face-centered cubic conventional cell $Cs_xCo_4[Fe(CN)_6]_y\cdot n'H_2O$, are reported in Table 1 where they are compared to the chemical formulas of the references **R1** and **R2**. In Table 1, taking into account the error bars in the stoichiometric coefficients, all the formulas correspond to neutral samples and indicates that no redox reactions involving external species different from Co or Fe occur. As the Cs/Fe ratio in the initial solutions increases, the amounts of cesium cation and $[Fe(CN)_6]$ entities in the conventional cell also increase. The correlation between the cesium cations and the $[Fe(CN)_6]$ entities

amounts along the series agrees with a progressive insertion of cesium cations in the tetrahedral sites of the face-centered cubic structure,[9,11,12] accompanied by the progressive filling of the $[Fe(CN)_6]$ vacancies O to compensate the charges. We have then a series of six compounds where the vacancies represent various quantities of the total iron sites: 32.5% for **R1**, 30% for **1**, 27.5% for **2**, 20% for **3**, 15% for **4**, and 2.5% for **R2**. As the amount of $[Fe(CN)_6]$ vacancies O in the structure decreases, the cobalt environment changes. The average cobalt atom environment is given by $CoN_{4.05}O_{1.95}$ in **R1**, $CoN_{4.2}O_{1.8}$ in **1**, $CoN_{4.35}O_{1.65}$ in **2**, $CoN_{4.8}O_{1.2}$ in **3**, $CoN_{5.1}O_{0.9}$ in **4**, and $CoN_{5.85}O_{0.15}$ in **R2** (N represents N-bonded cyanide, and O, the oxygen of a coordinated water molecule). In each case, of course, the figures are a mean representative of a distribution of cyanide ions and water molecules in the cobalt coordination sphere.

Infrared Spectroscopy. Over the cyanide vibration range, three bands are observed: the band at 2160 cm^{-1} is attributed to the cyanide stretching vibration mode in the $Fe^{III}-CN-Co^{II}$ entities; the band at 2120 cm^{-1} is attributed to the cyanide in the $Fe^{II}-CN-Co^{III}$ entities whereas the band at 2090 cm^{-1} is assigned to the cyanide in the $Fe^{II}-CN-Co^{II}$ entities.[13,14] Compound **R1**, mainly built of $Fe^{III}-CN-Co^{II}$ pairs exhibits essentially the sharp band at 2160 cm^{-1}, whereas **R2**, mainly built of $Fe^{II}-CN-Co^{III}$ pairs exhibits a wide band centered at 2120 cm^{-1}. The spectra of compounds **1**, **2**, **3**, and **4** exhibit the three bands, more or less broad and resolved. On the spectra of **1** and **2**, the three bands clearly appear. The spectrum of **3** exhibits a wide band centered at 2105 cm^{-1}, envelope of the $Fe^{II}-CN-Co^{III}$ and $Fe^{II}-CN-Co^{II}$ contributions. The shoulder at 2160 cm^{-1} is the signature of $Fe^{III}-CN-Co^{II}$ entities. The spectrum of **4** exhibits only one very broad band, envelope of the three cyanide contributions. From compound **1** to compound **4**, $Fe^{II}-CN-Co^{III}$ pairs progressively replace the $Fe^{III}-CN-Co^{II}$ ones. This change is correlated to the one of the cobalt environment, which goes from an average of $CoN_{4.2}O_{1.8}$ in **1** to an average of $CoN_{5.1}O_{0.9}$ in **4**. Due to the increasing ligand field around the cobalt atoms, the amount of spontaneous electron transfer $Fe^{III}-CN-Co^{II} \rightarrow Fe^{II}-CN-Co^{III}$ during the synthesis progressively increases from **R1** to **R2**, going through **1**−**4**. Furthermore, from **R1** to **4**, the IR bands broaden, probably due to an increase of the structural disorder induced by the simultaneous presence of cobalt atoms with different first neighbor bond-lengths in the structure. Indeed, for Co^{II} (HS) L_6 (L = O/N), the Co-L mean distance is around 2.08 Å,[10,15] whereas it is 1.91 Å for Co^{III} (BS) L_6 (L = O/N).[10,16,17] Besides, this band is not so broad in the spectrum of compound **R2**, which mainly contains $Fe^{II}-CN-Co^{III}$ pairs, that is to say a majority of Co−L short bonds.

X-ray Absorption Spectroscopy. X-ray absorption near edge structure (XANES) measurements at the Co (Figure 1) and Fe (Figure 2) K edges were performed to determine the oxidation states of the iron and of the cobalt ions in compounds **1**-**4** and their spectra compared to those of **R1** and **R2**.

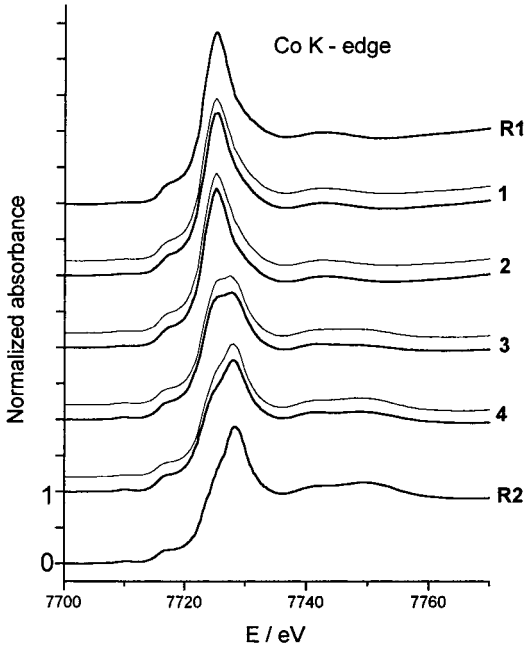

Figure 1. Co K edge XANES spectra of compounds **1**, **2**, **3**, **4**, **R1**, and **R2**; (bold-face line) experimental spectra, (light-face line) best linear combinations using the spectra of compounds **R1** and **R2**. For clarity, the absorbance of each experimental spectrum has been shifted by one and the computed spectrum by a further 0.2.

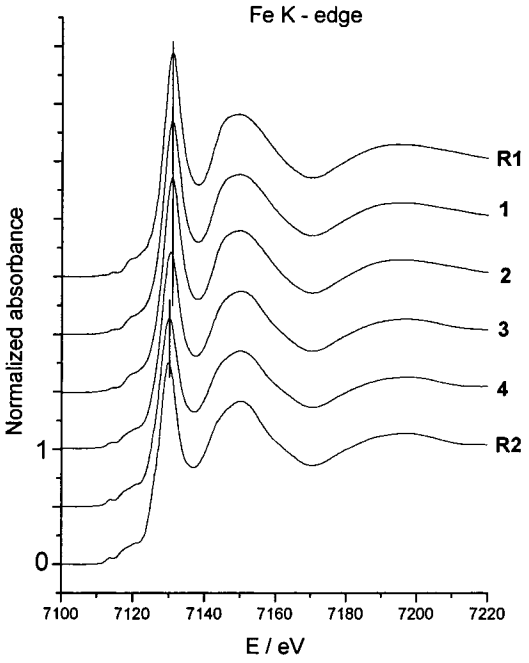

Figure 2. Fe K edge XANES spectra of compounds **1**, **2**, **3**, **4**, **R1**, and **R2**. The absorbance of each spectrum has been shifted by one-half for clarity.

The assignment of the main XANES features at the Co and Fe K edges and the analysis of the spectra of **R1** and **R2** were published in Part 1.[8] We have shown that **R1** mainly contains cobalt ions at the +II oxidation state and iron ions at the +III oxidation state, whereas **R2** mainly contains cobalt ions at the +III oxidation state and iron ions at the +II oxidation state.

Figure 1 shows that, at the cobalt K edge, the spectra of compounds **1**−**4** are intermediate between the reference spectra **R1** and **R2**. Qualitatively, the shift of the relative intensities of the absorption maxima intensities (7725 eV for Co^{II} ions and 7728 eV for Co^{III} ions) follows the progressive increase of

(11) Holmes, S. M.; Girolami, G. S. *J. Am. Chem. Soc.* **1999**, *121*, 5593−5594.
(12) Yamada, S.; Kuwabara, K.; Koumoto, K. *Mater. Sci. Eng. B* **1997**, *B49*, 89−94.
(13) Gadet, V. Ph.D. Thesis, Université Pierre et Marie Curie, Paris, France, 1992.
(14) Reguera, E.; Bertran, J. F.; Diaz, C.; Blanco, J.; Rondon, S. *Hyperfine Interact.* **1990**, *53*, 391−395.
(15) Giorgietti, M.; Berrettoni, M.; Filipponi, A.; Kulesza, P. J.; Marassi, R. *Chem. Phys. Lett.* **1997**, *275*, 108−112.
(16) Morales, A. D.; Romero, R. G.; Rodriguez, J. D.; Hernandez, R. P.; Bertran, J. F. *Transition Met. Chem.* **1990**, *15*, 106−108.
(17) Roux, C.; Adams, D. M.; Itié, J. P.; Polian, A.; Hendrickson, D.; Verdaguer, M. *Inorg. Chem.* **1996**, *35*, 2846−2852.

the Co^{III}/Co^{II} ratio in the structure as the amount of cesium cations per cell increases. Quantitatively, the edge spectra of the four compounds are fairly well reproduced by linear combinations of the corresponding spectra of **R1** and **R2**, representatives of the two electronic states expected for the Co ions in our materials. The best agreement (positions and intensities of the main features) between the experimental spectra and linear combinations of the two reference spectra are reported in Figure 1. The spectrum of **1** is reproduced by 95% of the spectrum of **R1** and 5% of the spectrum of **R2**. The best combinations of **R1** and **R2** spectra are respectively 85 and 15% for **2**, 40 and 60% for **3**, 15 and 85% for **4**. The uncertainty on the percentages is less than 5%.

Figure 2 shows the iron K edge spectra of compounds **1**−**4** compared to the ones of **R1** and **R2**. Going from **R1** to **R2**, we observe a 1 eV low-energy shift of the preedge and of the absorption maximum, due to the decrease of the oxidation state from mainly +III (compound **R1**) to mainly +II (compound **R2**). All the spectra resemble each other and are characteristic of the $[Fe(CN)_6]$ entity.[8,18,19]

The spectra of **1**, **2**, and **R1** are practically identical. The energy of the weak preedge (7114.5 eV) and of the absorption maxima (7131.0 eV for **R1**, 7130.7 eV for **1** and **2**) indicates that the oxidation state of iron ions is mainly +III for the three compounds. The spectrum of **3** is intermediate between those of **R1** and **R2**: the absorption maximum is at 7130.5 eV, between 7131.0 eV for **R1**, and 7130.0 eV for **R2**. The result indicates the simultaneous presence of Fe^{II} and Fe^{III} species in compound **3**. The energy position of the absorption maximum for compounds **4** and **R2** are the same: therefore, the iron is mainly at the +III oxidation state in **4**.

The difference between the two reference spectra is weaker at the iron K edge than at the cobalt K edge due to the real charge on the iron ion well-known to be close for the two oxidation states since the overall charge is spread over the six cyanide ligands.[8,18,19] So, the linear combinations of the **R1** and **R2** spectra reproducing the intermediate spectra **1**−**4** confirm the results at the Co K edge, but with a larger uncertainty and they are not presented here.

The results confirm the electron transfer leading to the formation of $Co^{III}-Fe^{II}$ diamagnetic pairs during the synthesis provoked by the increase of the ligand field Δ_{Co} around the cobalt controlled by Cs insertion along the series.[8]

X-ray Powder Diffraction. The powder diffraction patterns of **1**−**4** are shown in Figure 3 where they are compared to those of **R1** and **R2**.

All the diffractograms are characteristic of a face-centered cubic structure,[8,11,12] but all are different. The position, half line-width and intensity of the reflections vary with the amount of alkaline cation in the structure. Given the important difference between the cell parameters of the extreme phases **R1** and **R2** (0.35 Å), one could expect, depending on the synthesis conditions, a phase demixtion into those two extreme phases which would lead to well resolved reflections. It is not the case here. For each reflection, only one peak appears. Furthermore, when the tetrahedral interstitial sites are progressively filled by the cesium ions, it is expected that the scattering of the metal atoms and of the alkali cations which is in phase for the 220 and 400 reflections and out of phase for the 200 and 420 reflections should lead to the relative increase of the intensity of the former reflections to the detriment of the latters.[8] This is

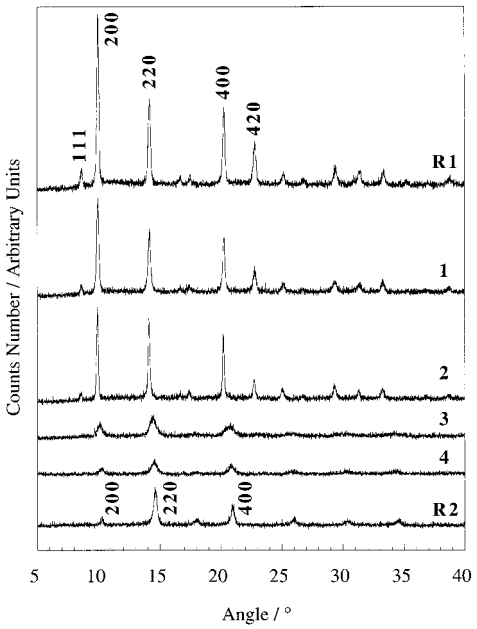

Figure 3. X-ray powder diffraction patterns of compounds **1**, **2**, **3**, **4**, **R1**, and **R2**.

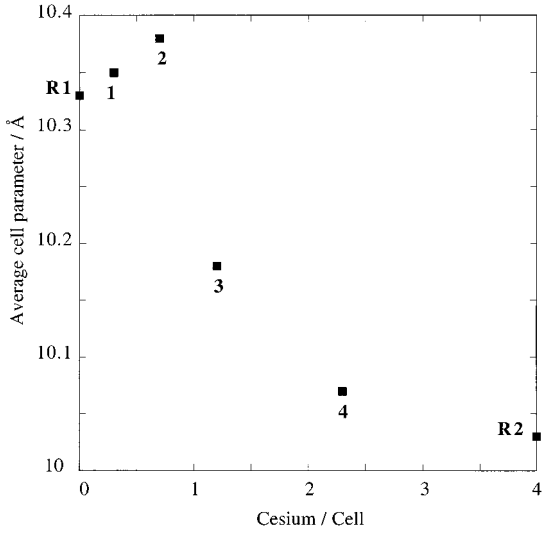

Figure 4. Average cell parameter of compounds **1**, **2**, **3**, **4**, **R1**, and **R2** as a function of cesium per unit cell.

experimentally observed and clearly confirms the progressive insertion of the cesium cations in the tetrahedral sites along the series **R1, 1**−**4, R2**.

The peaks, narrow and intense for low cesium cations content (in **R1**, **1**, and **2**) broaden and collapse (in **3** and **4**), which expresses a decrease of the long-range order as the amount of inserted cesium cation increases. They narrow and grow again in **R2**, which reflects on the contrary, a gain of long-range order for the highest cesium cations content. This trend is in agreement with the broadening of the IR bands along the series and can be attributed to the simultaneous presence of cobalt atoms with different cobalt first neighbor bond-length.

The position of the 200, 220, and 400 reflections have been determined for all the compounds and an average unit cell parameter, *a*, has been calculated. Its values as a function of the Cs amount per cell in the compounds are reported in Figure 4.

The cell parameters of **R1** and **R2** directly reflect the electronic state of the cobalt atoms in the structures: $Co^{II}HS$

(18) Yokoyama, T.; Ohta, T.; Sato, O.; Hashimoto, K. *Phys. Rev. B* **1998**, *58*, 8257−8266.
(19) Bianconi, A.; Dell'Ariccia, M.; Durham, P. J.; Pendry, J. B. *Phys. Rev. B* **1982**, *26*, 6502−6508.

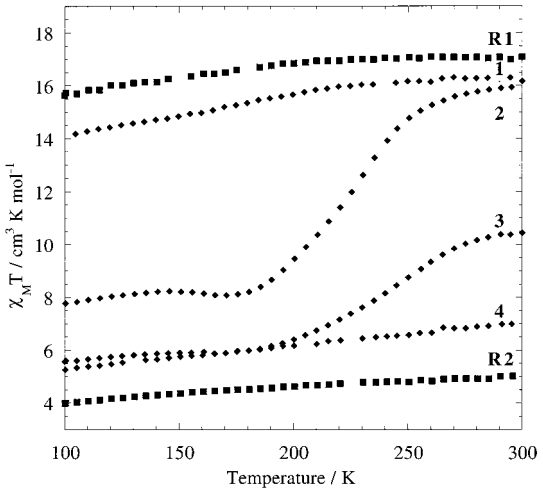

Figure 5. Plot of the product of the molar magnetic susceptibility times temperature vs temperature for compounds **1**, **2**, **3**, **4**, **R1**, and **R2**.

with long coordination bonds in **R1** ($a = 10.35 \pm 0.05$ Å), Co^{III}LS with short coordination bonds in **R2** ($a = 10.00 \pm 0.05$ Å).[8]

From 0 to 0.7 cesium cation per cell, the average cell parameter increases. It is well-known that the insertion of large cations such as cesium in the tetrahedral sites of the fcc structure of Prussian blue analogues produces such an increase of the cell parameter, everything else remaining unchanged.[11,13,20,21] This is the prevailing effect at low cesium content.

From 0.7 to 4 cesium cations per cell, the average cell parameter progressively decreases, with a stronger slope between 0.9 and 2. This variation reflects the progressive transformation of Co^{II} (HS) species in Co^{III} (LS) species in the structure and the corresponding average decrease of Co-ligands length.

Magnetism and Photoinduced Magnetization. The temperature dependence of $\chi_M T$ (T = temperature, χ_M = molar magnetic susceptibility, M = molecular weight of the formula units of Table 1) relative to **R1**, **1**−**4**, and **R2** over the 100−300 K temperature range is shown in Figure 5. The temperature range is limited to the paramagnetic area of interest.

R1 and **R2** exhibit a nearly constant $\chi_M T$ value over the paramagnetic temperature range. As expected for the powder containing the highest quantity of paramagnetic centers, compound **R1** exhibits the highest $\chi_M T$ value. The $\chi_M T$ value for compound **R2**, we thought essentially composed of diamagnetic pairs, is not close to zero. This shows that compound **R2** contains a non-negligible amount of paramagnetic entities Co^{II} and Fe^{III}. To evaluate this amount, $\chi_M T$ cannot be computed from a spin only contribution. Thus, the Curie constants of Co^{II} and Fe^{III} in analogous environments have been extracted by a linear fit of $1/\chi_M$ versus T over the 100−300 K temperature range for two Prussian blue analogues, standards with chemical formula $Co^{II}_4[Co^{III}(CN)_6]_{2.7}\cdot 17H_2O$ where only Co^{II} ions are paramagnetic and $Zn^{II}_4[Fe^{III}(CN)_6]_{2.7}\cdot 18H_2O$ where only Fe^{III} ions are paramagnetic. We obtained $C_{Co}{}^{II} = 3.15$ cm^3 mol^{-1} from the first standard and $C_{Fe}{}^{III} = 0.95$ cm^3 mol^{-1} from the second one close to the previously determined values.[22,23] As **R2** is neutral and as the change in the oxidation states of the metal cations exclusively comes from an internal redox process during the synthesis, the paramagnetic entities must come from an incomplete electron transfer during the synthesis. The Co/Fe ratio being close to 1 in **R2**, the Curie constant per cell (5.6 cm^3 mol^{-1}) compared to $C_{Co}{}^{II}$ and $C_{Fe}{}^{III}$, gives 34% of Co^{II}−Fe^{III} paramagnetic pairs in **R2**, considering the exchange as negligible.

The intermediate compounds exhibit very different magnetic behaviors. For **1**, the $\chi_M T$ value is high, close to the $\chi_M T$ value of the reference compound **R1** and decreases slightly over the whole temperature range. For **2** and **3**, $\chi_M T$ is practically constant from 300 to 280 K, then significantly decreases from 280 to 170 K and then slightly under 170 K. The magnetization value at 300 K before and after the measurement was the same. For **4**, the $\chi_M T$ value is low, close to the one of **R2**, and decreases slightly over the considered temperature range.

At 300 K, $\chi_M T$ of the different samples decreases as the cesium content increases, which reflects the increasing electron transfer which occurs during the synthesis and gives an increasing amount of diamagnetic pairs along the series.

We attribute the variation of $\chi_M T$ as a function of the temperature, between 280 and 170 K, for **2** and **3** to a thermally induced electron transfer:

$$Co^{III}-NC-Fe^{II} \underset{T\downarrow}{\overset{T\uparrow}{\rightleftharpoons}} Co^{II}-NC-Fe^{III}$$

This electron transfer was already observed by Hashimoto and co-workers.[18] It is induced by the effect of temperature on the cobalt(II) ions which present an intermediate ligand field. This phenomenon deserves a particular study which will be presented elsewhere. A similar phenomenon occurs in the molecular complex $Co^{II}(bipy)(semiquinone)_2\cdot$solvent synthesized by Hendrickson.[24,25]

For a cesium content per cell less than 0.3, the average ligand field around the cobalt ion is not strong enough to produce, combined with the temperature, this thermally induced electron transfer. For a cesium content per cell between 0.7 and 1.2, some of the Co(II) ions are implied in a chemically induced electron transfer, during the synthesis at 300 K. When the samples are cooled, some other cobalt(II) ions undergo a thermally induced electron transfer. The magnitude of the phenomenon depends on the ligand field around the cobalt and therefore on the amount of cesium cations in the structure. The $\chi_M T$ values at 300 K are different in **2** and **3** because the Co^{II}/Co^{III} ratios are different. The low temperature $\chi_M T$ values are also different which indicates that the thermally induced electron transfer is not total. However, the temperature range of the electron transfer is close for both compounds and spread out. This is a strong indication that the kind of pairs involved in the thermally induced electron transfer is the same in both compounds. Furthermore, if the analogy with molecular spin crossover systems[26−28] can be done, the wide temperature range of the transition would indicate a weak cooperativity of the phenomenon. For a cesium content per cell more than 2.1, the chemically induced electron transfer during the synthesis is not total, and no further thermally induced electron transfer occurs upon cooling.

The magnetization under irradiation at 10 K as a function of irradiation time is shown in Figure 6. The thermal variation of

(20) Gadet, V.; Mallah, T.; Castro, I.; Verdaguer, M.; Veillet, P. *J. Am. Chem. Soc.* **1992**, *114*, 9213−9214.
(21) Griebler, W.-D.; Babel, D. *Z. Naturforsch.* **1982**, *37b*, 832−837.
(22) Figgis, B. N.; Lewis, J. *Progress in Inorganic Chemistry*; Interscience: New York, 1964.
(23) Baker, J.; Figgis B. N., *J. Chem. Soc., Dalton Trans*. **1975**, 598.
(24) Adams, D. M.; Dei, A.; Rheingold, A. L.; Hendrickson, D. N. *Angew. Chem., Int. Ed. Engl.* **1993**, *32*, 880−882.
(25) Lynch, W. M.; Valentine, M.; Hendrickson, D. N. *J. Am. Chem. Soc.* **1982**, *104*, 6982−6989.
(26) Gütlich, P.; Garcia, Y.; Goodwin, H. A. *Chem. Soc. Rev.* **2000**, 419−427.
(27) Gütlich, P.; Hauser, A.; Spiering, A. *Angew. Chem., Int. Ed. Engl.* **1994**, *33*, 2024−2054.
(28) Toftlund, H. *Coord. Chem. Rev.* **1989**, *94*, 67−108.

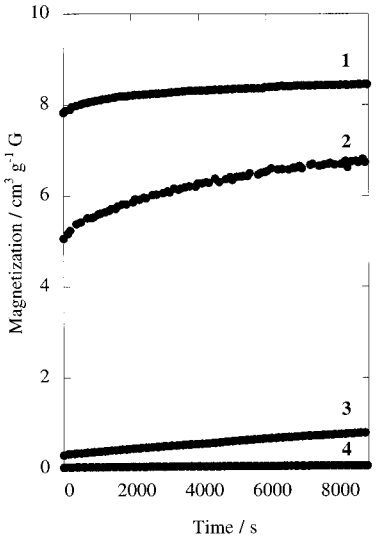

Figure 6. Magnetization M under irradiation at 10 K vs time of irradiation in compounds **1**, **2**, **3**, and **4**, in a field $H = 500$ G.

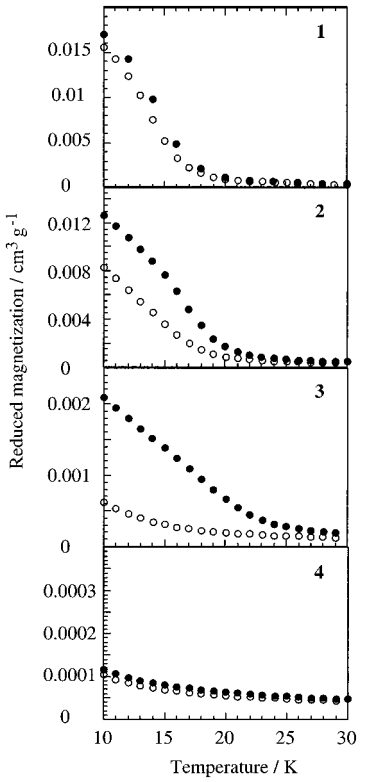

Figure 7. Reduced Magnetization (M/H) per gram of compounds **1**, **2**, **3**, and **4** as a function of temperature before (○) and after (●) irradiation over the 10−30 K temperature range. For clarity, the ordinate scales are different for the four compounds.

the reduced magnetization before and after irradiation of **1**−**4** is shown in Figure 7 over the 10−30 K temperature range.

The initial magnetization (Figure 6, $t = 0$) strongly decreases from **1** to **4**. This reflects the progressive decrease of the number of paramagnetic centers along the series and the progressive loss of three-dimensional magnetic order. Furthermore, the magnetization profile under irradiation as a function of time (Figure 6) progressively evolves from **1** to **4**. The magnetization of compounds **1** and **2** rapidly increases to reach a plateau for **1** and to nearly reach a plateau for **2**. A spin-allowed excited-state relaxes (by intersystem crossing) to the high spin Fe^{III}−Co^{II} metastable magnetic state with longer cobalt first-neighbor bonds. Indeed, the inorganic network, containing an important amount of $[Fe(CN)_6]$ vacancies □, is flexible and allows the bond lengthening. The transformable diamagnetic pairs are rapidly transformed in their magnetic metastable counterparts. A longer exposure to light does not lead to a further increase of the magnetization. On the contrary, the increase of the magnetization is much slower in **3** and even slower in **4**. It continuously increases over the whole irradiation time. A longer exposure to light would then lead to a further increase of the magnetization. The relaxation of the spin allowed excited state to the metastable magnetic state appears more difficult than before. Indeed, the bond lengthening around the cobalt, easy when the inorganic network contains enough $[Fe(CN)_6]$ vacancies □, which give some flexibility to the network, becomes more and more difficult when the $[Fe(CN)_6]$ vacancies □ amount are disappearing. Although compound **4** contains the largest amount of diamagnetic pairs, the magnetization remains low since the structure, which contains few $[Fe(CN)_6]$ vacancies □, undergoes strong network strains which impede the trapping of the metastable state.

Before irradiation, **1** is ferrimagnetic under 17 K (Figure 7), very close to the Curie temperature of the Prussian blue analogue free from alkali cations (around 16 K). After irradiation, the magnetic behavior of the compound is nearly the same, the magnetization is slightly higher with a ratio of the magnetization after irradiation (M_A in the following) over the magnetization before irradiation (M_B in the following) at 10 K of $M_A/M_B = 1.1$, which reveals a weak photoexcitation efficiency, due to the weak amount of Co^{III}−Fe^{II} diamagnetic pairs in the sample.

Before irradiation, compound **2** is clearly less magnetized than compound **1**. The important difference of behavior between compound **1** and compound **2** (even if they are very close at 300 K), arises from the electron transfer occurring upon cooling and leading to an important amount of Co^{III}−Fe^{II} diamagnetic pairs in **2**. After irradiation, **2** becomes ferrimagnetic with a Curie temperature around 19 K, which reflects, compared to compound **1**, the increase of magnetic neighbors associated to the stoichiometry. The M_A/M_B ratio of 1.3 at 10 K is higher than in compound **1** due to the presence of more Co^{III}−Fe^{II} "efficient" diamagnetic pairs. We call "efficient" diamagnetic pairs Co^{III}−Fe^{II} entities where the cobalt is in a flexible enough environment to reach the metastable magnetic state when excited by light.

Compound **3** is paramagnetic before irradiation with a low magnetization compared to **1** and **2** due to the higher content of diamagnetic pairs. After irradiation, the magnetization versus temperature of **3** displays a paramagnetic contribution and a ferrimagnetic one. The M_A/M_B ratio of 3.5 at 10 K is much higher than in the previous compounds.

Compound **4** is slightly paramagnetic before and after irradiation. The M_A/M_B ratio at 10 K is equal to 1.2. The compound does not present a significant photomagnetic effect. Even if the amount of Co^{III}−Fe^{II} diamagnetic pairs is maximum in this compound, the network strains prevent their trapping in a metastable well.

The photoinduced electron transfer is thermally reversible in all of the studied compounds of this Prussian blue analogue family.[5,29] Back to room temperature, the compounds recover their initial magnetization. The relaxation temperature of the metastable photoinduced state can be defined as the temperature at which the magnetization of the sample becomes the same as the one before irradiation. When the photoinduced magnetization is weak (**1** and **4**), the magnetization curves before and after

(29) a) Goujon, A.; Roubeau, O.; Varret, F.; Dolbecq, A.; Bleuzen, A.; Verdaguer, M. *Eur. Phys. J. B*, **2000**, *14*, 115−124. (b) Goujon A. et al., Proceedings of ICMM2000, *Polyhedron* **2001**. In press.

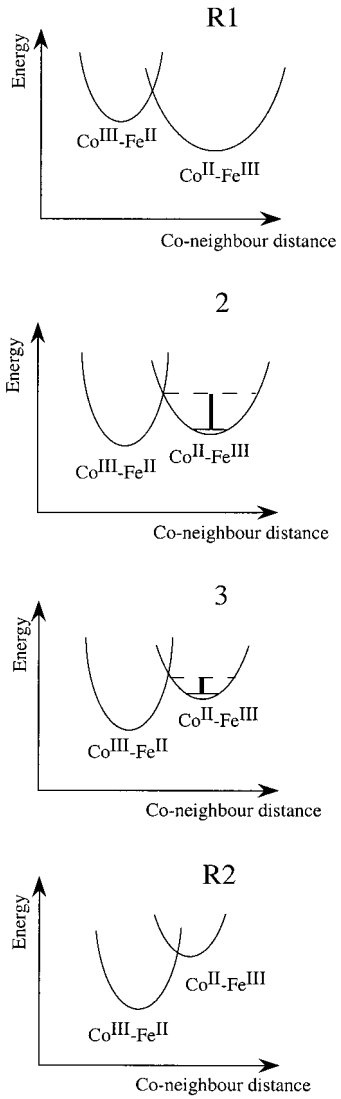

Figure 8. Schematic potential energy wells in compounds **2**, **3**, **R1**, and **R2**.

irradiation are nearly superimposed which makes the determination of the relaxation temperature difficult. For compounds **2** and **3**, the relaxation temperatures of the excited state are 160 ± 5 and 140 ± 5 K, respectively. The difference is beyond the experimental uncertainty. Two reasons illustrated by schematic representations of the mean ground and metastable states wells for compound **R1**, **2**, **3**, and **R2** (Figure 8) may explain the observed difference.

First, it is well-known in the field of spin crossover systems, that an increase of the ligand field strength, here the average ligand field around the cobalt atom, essentially produces an energy shift of the potential wells of the ground and of the metastable states. In the present case, a stronger Δ_{Co} stabilizes the $Co^{III}-Fe^{II}$ ground state as in **R2** (Figure 8) and, on the contrary, destabilizes the $Co^{II}-Fe^{III}$ state. Then, a stronger Δ_{Co} should lower the thermal energy barrier between the photoinduced metastable state and the ground state and therefore the relaxation temperature.

Second, in a three-dimensional compound undergoing strong network strains, the reduction of the network flexibility, that is the decrease of the number of $[Fe(CN)_6]$ vacancies □, may prevent the metastable excited state to reach the strainless equilibrium position. The $Co^{II}-L$ bonds in the excited state would be shorter. The flexibility reduction would then translate the metastable excited-state potential to the left toward the ground-state one and would narrow it. The flexibility reduction may then also lower the thermal energy barrier between the metastable photoinduced state and the ground state, and once more, the relaxation temperature.

Theoretical study and calculations have been undertaken by Kawamoto et al. to determine the potential wells positions.[30]

Table 2. Amounts of the Various Cations in a Conventional Unit Cell and Percentages of Co^{III} and Co^{II} in Compounds **1**−**4** and **R1**, **R2**, **R3** Obtained from Chemical Analysis and the Best Linear Combinations of XANES Reference Spectra

sample	Cs^+	Co^{2+}	Fe^{3+}	$Co^{3+} = Fe^{2+}$ [a]	Co^{3+} (%)	Co^{2+}(%)
R1	0	4	2.70	0	0	100
1	0.3	3.90	2.70	0.10	3	97
2	0.7	3.58	2.48	0.42	12	88
3	1.2	2.30	1.50	1.70	43	57
4	2.3	1.62	1.02	2.38	60	40
R2	3.9	1.20	1.10	2.80	70	30
R3[b]	1.8	0.7	0	3.3	82.5	17.5

[a] Electron transfer at 300 K. [b] In **R3**, the alkali cation (1.8) is Rb^+ instead of Cs^+.

Discussion and Conclusions

Compound **R2**, which contains the maximum of cesium cations is mainly composed of cobalt atoms at the oxidation state +III and iron atoms at the oxidation state +II. However its $\chi_M T$ value shows that it still contains paramagnetic entities. The comparison of the $\chi_M T$ value to standard compounds leads to Co^{II}/Co^{III} ratio of 34/66. In part 1,[8] we synthesized $Rb_{1.8}Co_4[Fe(CN)_6]_{3.3}\cdot 13H_2O$, compound **R3**, also mainly composed of Co^{III} and Fe^{II}. Due to the stoichiometry, the percentage of cobalt ions remaining at the +II oxidation state represents at least 17.5% of the total cobalt sites in **R3**. It is possible to reproduce the Co K edge XANES spectrum of compound **R2** by a linear combination of 15% of **R1** spectrum (Co^{III}/Co^{II} = 0/100) and 85% of **R3** spectrum. Assuming a total electron transfer in **R3** (Co^{III}/Co^{II} = 82.5/17.5), the Co^{III}/Co^{II} ratio in compound **R2** would be 30/70, very close to the 34/66 determined by magnetic measurements.

The higher electron transfer occurring in compound **R3** compared to the one in compound **R2** can be attributed to a higher Δ_{Co} in the former compound due to the smaller size of the inserted alkali cation. The parameter cell is actually slightly lower in **R3** (9.98 ± 0.05 Å) than in **R2** (10.03 ± 0.05 Å). The difference could also depend on the behavior of the different alkali cations, rubidium and cesium, during the condensation process (electrostatic effects, ion pairing, etc.).

Knowing the percentages of Co^{III} and Co^{II} in compounds **R1** and **R2**, it is possible to evaluate them in all the compounds of the series using the XANES linear combinations presented in Figure 1. The calculated values are reported in Table 2. The variation of the amount of $[Fe(CN)_6]$ vacancies □ and the electron transfer per cell which occurs during the synthesis at 300 K as a function of the cesium content per cell are reported in Figure 9.

Whereas the change of the iron vacancies amount varies linearly because of simple electrostatic compensation, the amount of electron transfer induced during the synthesis as a function of the cesium content present sigmoid shape. The electron-transfer process is complex and depends on several parameters:

(i) the increase of the cell parameter due to the insertion of the cesium cation leading to a decrease of Δ_{Co}, the cobalt-ligand bonds being longer,

(30) Kawamoto, T.; Asai, Y.; Abe, S. *Phys. Rev. B* **1999**, *60*, 12990−12993.

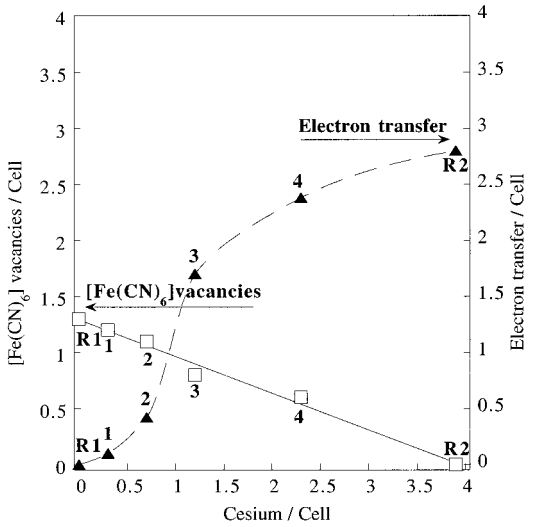

Figure 9. Amount of $[Fe(CN)_6]$ vacancies (□) and electron transfer (▲) per unit cell at 300 K in compounds **1**, **2**, **3**, **4, R1**, and **R2** as a function of the cesium content per unit cell.

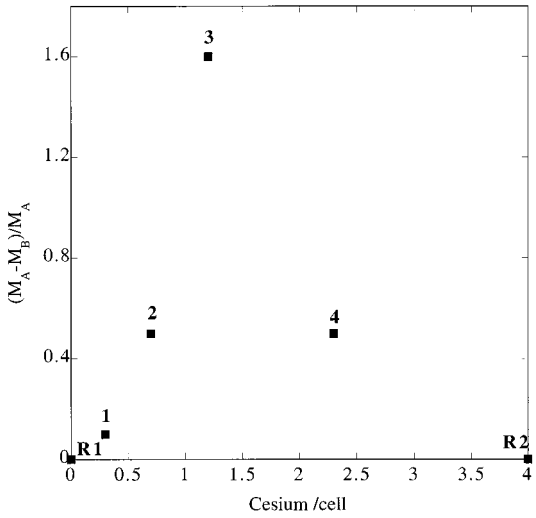

Figure 10. $(M_A - M_B)/M_A$ ratio at $T = 10$ K vs the cesium content per unit cell. M_A is the magnetization after irradiation, and M_B, the magnetization before irradiation.

(ii) the increase of the number of N-bonded cyanides around the cobalt, leading on the contrary to an increase of Δ_{Co}.

Furthermore, the role of the alkali cation in solution during the elaboration of the inorganic network (electrostatic effects, ion pairing, etc.) is probably not innocent.

Given the percentages of the cobalt atoms of different oxidation states and the different coordination bond-lengths, the correlation between them and the structural parameters clearly appears. The compounds with the less organized long-range order are the closest of the $Co^{III}/Co^{II} = 50/50$ composition. Compounds **R1**, **1**, and **2** contain less than 10% of Co^{III}, the diffraction patterns exhibit intense and narrow peaks. Compounds **3** and **4** are close to the mean composition (50/50), $Co^{III}/Co^{II} = 43/57$ and $Co^{III}/Co^{II} = 60/40$, respectively, and their diffraction patterns exhibit very weak and broad peaks. **R2** exhibits a more resolved diffraction pattern in agreement with the ratio $Co^{III}/Co^{II} \approx 70/30$. **R3** which corresponds to the ratio $Co^{III}/Co^{II} = 82/18$ displays again more intense and narrower diffraction lines.[8] The decrease of long-range order is directly linked to the relative amount of Co^{II} and Co^{III} in the structure and reflects the difficulty for the fcc structure to simultaneously accommodate Co^{II} with long coordination bonds and Co^{III} with short coordination bonds. The powder diffraction results confirm the absence of two different phases in the compounds.

The efficiency of the photomagnetism may be expressed by the ratio $(M_A - M_B)/M_A$ where M_A and M_B are the magnetizations at 10 K after and before irradiation, respectively. The values of this ratio as a function of cesium cation content per cell are presented in Figure 10.

Figure 10 clearly shows that the most efficient compound of the series is **3** and that the most efficient compound probably is intermediate between **3** (1.2 Cs per cell) and **4** (2.3 Cs per cell). Accordingly, **R3**, which is also very efficient,[8] contains 1.8 rubidium per cell, which lies in the above range, 1.2−2.3 alkali cations per cell. Furthermore, the relaxation temperature of the excited metastable state in **R3** (110 K)[29] or a similar compound (120 K) synthesized by Sato and co-workers[5] is lower than the ones of **2** and **3** in agreement with a stronger Δ_{Co} and a less flexible structure (17.5% of $[Fe(CN)_6]$ vacancies). The results clearly show that the efficiency of the photoinduced process depends above all on a compromise between the amount of $Co^{III}-Fe^{II}$ diamagnetic pairs and the amount of $[Fe(CN)_6]$ vacancies □ providing the network flexibility which allows the trapping of the photoinduced metastable state. This family of compounds unambiguously evidenced the fundamental role of the intrinsic $[Fe(CN)_6]$ vacancies □ which can also be of interest for the dynamics of the magnetization not dealt with here.[32,33]

Furthermore, we control through this series a thermally induced electron transfer already observed by Hashimoto.[18] For low alkali cations insertion, Δ_{Co} is weak, and the Co^{II} ions remain essentially high spin, whatever the temperature. By slightly increasing the alkali cations content, $|\Delta_{Co} - P|$ (where P is the pairing energy) becomes close to the thermal energy kT, so that a further amount of cobalt atoms can undergo a spin change accompanied by an electron transfer to $[Fe(CN)_6]$ upon cooling. For high alkali cations insertion rates, Δ_{Co} is the strongest, and the Co atoms remain essentially low spin at the +III oxidation state, whatever the temperature. Such transition is a classical phenomenon observed in spin crossover[27,28] or valence tautomerism[24,25,31] compounds. The new features in these systems are the following:

(1) The compounds are three-dimensional; metal atoms are chemically linked in the three directions of space through short −CN− bridges.

(2) The strength of the ligand field is controlled by the ratio of two ligands (H_2O− weak field and N-bonded CN− stronger field) linked to the cobalt atom.

(3) The spin crossover of the Co(II) is accompanied by a metal−metal electron transfer.

An internal strain, the chemical insertion of alkali cations, and an external strain, temperature, then modify the magnetic properties of the compounds.

Acknowledgment. We thank the European Community (Grant ERBFMRXCT980181), Contract TMR/TOSS (FMRX-CT98-0199), European Science Foundation (Molecular Magnets), and CNRS (Program Matériaux) for financial support.

Supporting Information Available: Infrared spectra of compounds **1-4**, **R1**, and **R2** (PDF). This material is available free of charge via the Internet at http://pubs.acs.org.

JA011296R

(31) Jung, O.-S.; Pierpont, C. G. *Inorg. Chem.* **1994**, *33*, 2227−2235.
(32) Pejacovic, D. A.; Manson, J. L.; Miller, J. S. *J. Appl. Phys.* **2000**, *87*, 6028−6030.
(33) Pejacovic, D. A.; Manson, J. L.; Miller, J. S.; Epstein, A. J. *Phys. Rev. Lett.* **2000**, *85*, 1994−1997.